

# Thermal behaviour of rocks

Authors: Prof. Dr. habil. Heinz Konietzky & M. Sc. Fei Wang  
(TU Bergakademie Freiberg, Geotechnical Institute)

---

1	Introduction.....	2
2	Basic laws and parameters .....	4
3	Lab test results .....	5
	3.1 Crack initiation and propagation.....	5
	3.2 Density .....	5
	3.3 Uniaxial compressive strength (UCS) .....	6
	3.4 Tensile strength.....	7
	3.5 Cohesion and friction angle.....	7
	3.6 Young's modulus and Poisson's ratio .....	8
	3.7 Linear thermal expansion coefficient.....	9
	3.8 Specific heat capacity .....	10
	3.9 Thermal conductivity .....	10
4	Applications .....	12
	4.1 Thermo-mechanical coupled modelling of granite specimen .....	12
	4.2 Thermo-mechanical coupled behaviour of heated porous rock sample .....	15
	4.3 Example: Thermo-mechanical coupled behaviour of a rock sculpture .....	16
	4.4 Thermo-mechanical coupled simulation of high-level waste storage facility .....	17
	4.5 Thermo-mechanical simulations of rock behaviour for underground coal gasification .....	17
	4.6 Thermo-mechanical behaviour of rock salt .....	17
5	References .....	19

## 1 Introduction

Temperature and heat flow, respectively, can have a significant impact on the behaviour of rock and rock masses. One can distinguish two different directions starting from room temperature (20 °C):

- Temperature decrease, becoming important if temperature falls below zero (freezing point of water)
- Temperature increase (all values above 20 °C)

This e-book chapter treats only the second case: rock behaviour at elevated temperatures.

When rocks are exposed to elevated temperatures, they are damaged by thermal cracking which is caused by the accumulation of internal stresses. Many researchers (e.g. Chen and Wang, 1980; Heap et al., 2013) have found that thermal stresses are mainly controlled by

- (a) the constituents of the rocks (minerals and pore fillings have different thermal expansion characteristics, see Tab. 1),
- (b) thermal expansion anisotropy within individual minerals and,
- (c) thermal gradients.

Also important are the boundary conditions. The induced damage leads to reduced strength and stiffness values. The reaction of rocks and rock masses due to thermal impacts are important for several geo-engineering projects or tasks, for instance:

- Deep geothermal energy
- Deep mining
- Petroleum engineering
- High-level nuclear waste storage
- Cutting and drilling processes as well as novel rock excavation methods
- Solar heating of rock monuments and buildings
- Fires in tunnels, mines and buildings

Tab. 1: Linear thermal expansion coefficients for selected minerals (Siegesmund et al. 2011)

Mineral	Linear thermal expansion coefficient		Temp. range [°C]
	Parallel to c-axis [K <sup>-1</sup> ]	Perpendicular to c-axis [K <sup>-1</sup> ]	
Calcite	$25.1 \times 10^{-6}$	$-5.6 \times 10^{-6}$	0-85
Dolomite	$25.8 \times 10^{-6}$	$6.2 \times 10^{-6}$	24-700
Quartz	$7.7 \times 10^{-6}$	$13.3 \times 10^{-6}$	0-80
Albite	$10.5 \times 10^{-6}$	$5.6 \times 10^{-6}$	25-970
Gypsum	$54 \times 10^{-6}$	$7-117 \times 10^{-6}$	25-42
Micas	$8.7 \times 10^{-6}$	$17.8 \times 10^{-6}$	unknown
Clay	$6 \times 10^{-6}$	$15 \times 10^{-6}$	25-350

## 2 Basic laws and parameters

Basic parameters for thermal calculations are:

- Temperature ( $T$ ) [K]
- Specific heat (capacity) ( $c$ ) [ $\text{J}\cdot\text{kg}^{-1}\cdot\text{K}^{-1}$ ]
- Thermal conductivity ( $k$ ) [ $\text{W}\cdot\text{m}^{-1}\cdot\text{K}^{-1}$ ]
- Heat flux ( $q$ ) [ $\text{W}\cdot\text{m}^{-2}$ ]
- Thermal diffusivity ( $\kappa$ ) [ $\text{m}^2\cdot\text{s}^{-1}$ ]
- Thermal expansion coefficient ( $\alpha$ ) [ $\text{K}^{-1}$ ]

Heat is the amount of energy flowing from a warmer object to one with lower temperature. Specific heat is the amount of heat per unit mass required to increase the temperature by one degree Kelvin. The thermal diffusivity describes the transfer rate of heat from a warmer to a colder object. Heat flow in rocks can be performed by conduction (heat is carried by solid constituents of the rocks) and/or convection (heat is carried by fluid flow inside the rock). The governed equation for heat conduction (also applicable for convection) is Fourier's law (product of thermal conductivity tensor and temperature gradient [ $\text{K}\cdot\text{m}^{-1}$ ]):

$$q_i = k_{ij} \cdot \nabla T_j \quad (1)$$

For connective boundary condition,  $q_n$  is the component of the flux normal to the boundary in the direction of the exterior normal,  $h$  is the convective heat-transfer coefficient [ $\text{W} / (\text{m}^2\cdot\text{K})$ ]:

$$q_n = h(T - T_e) \quad (2)$$

Temperature increase can produce, depending on boundary conditions, additional stresses and/or strains according to the following equations ( $K$  = bulk modulus):

$$\Delta\sigma_{ij} = \delta_{ij} \cdot 3 \cdot K \cdot \alpha \cdot \Delta T \quad (3)$$

$$\Delta\varepsilon_{ij} = \delta_{ij} \cdot \alpha \cdot \Delta T \quad (4)$$

Thermal diffusivity – a measure for heat transfer rate - is defined as follows:

$$\kappa_{ij} = \frac{k_{ij}}{\rho \cdot c} \quad (5)$$

### 3 Lab test results

#### 3.1 Crack initiation and propagation

Microscopic observations have shown that more and more thermal microcracks will occur with increasing temperature as Fig. 3.1 indicates. Thermal induced cracks lead to modifications of the mechanical properties with increasing temperature as documented in the following chapters.

#### 3.2 Density

Density of rocks decreases with increasing temperature due to volumetric expansion and the release of volatile matter (mass loss) (Otto and Kempka 2015). Exemplary, Fig. 3.2 shows that the decrease of granite density up to 1000 °C is relatively small compared with the values at room temperature.

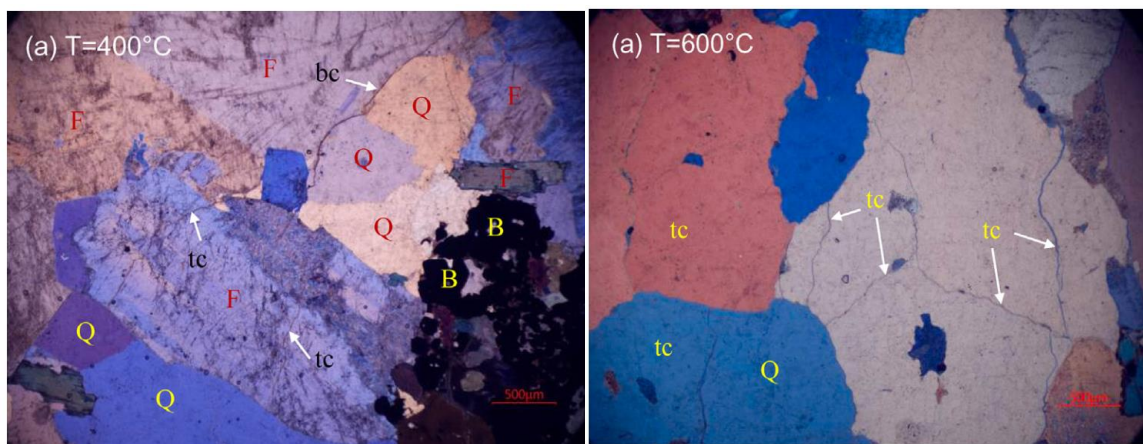


Fig. 3.1 Optical microscopic observations of thermal induced microcracks in granite specimens, bc - boundary crack, tc - transgranular crack, F - Feldspar, Q – Quartz and B - Biotite (Yang et al., 2017)

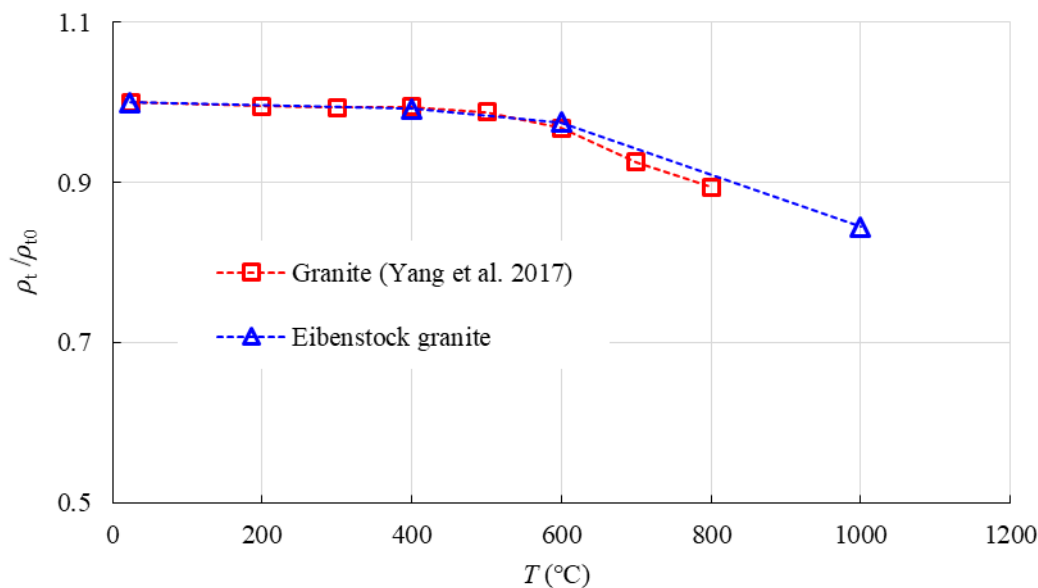


Fig. 3.2 Normalized bulk density vs. temperature for granite samples

### 3.3 Uniaxial compressive strength (UCS)

The trend of UCS change is complex at elevated temperatures, although it is more likely to decrease with increasing temperature. As shown in Fig. 3.3 and Fig. 3.4, different rocks including sandstone, marble and granite show different patterns. Even for the same type of rocks the strength development can be different.

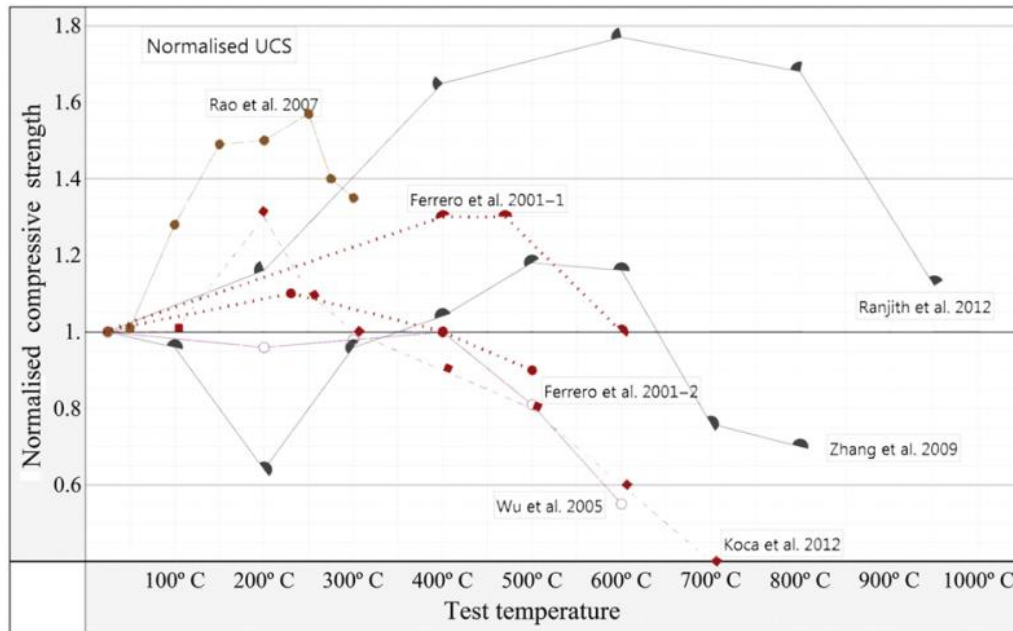


Fig. 3.3 Normalized UCS of different types of rocks vs. temperature (Brotóns et al., 2013)

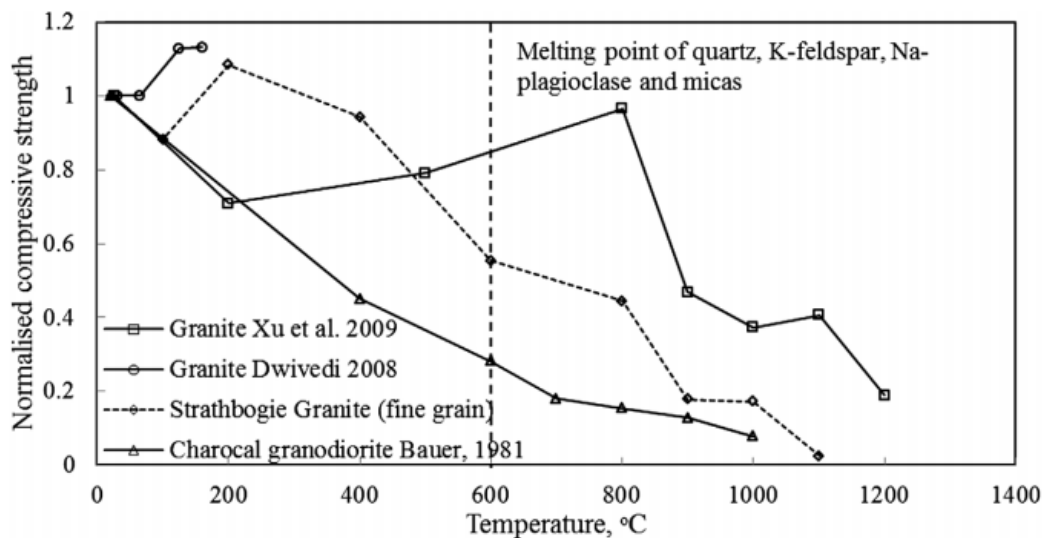


Fig. 3.4 Normalized UCS of granite samples vs. temperature (Shao et al., 2015)

### 3.4 Tensile strength

For most rocks, tensile strength will decrease with increasing temperature, especially after 400°C where the decreasing rate becomes much higher (fig. 3.5). However, for some rocks like Patrik granite in fig. 3.5, the tensile strength evolves in a non-monotonic manner with temperature. Guha Roy & Singh (2016) showed that the decrease of tensile strength of granite is negligible below 250 C.

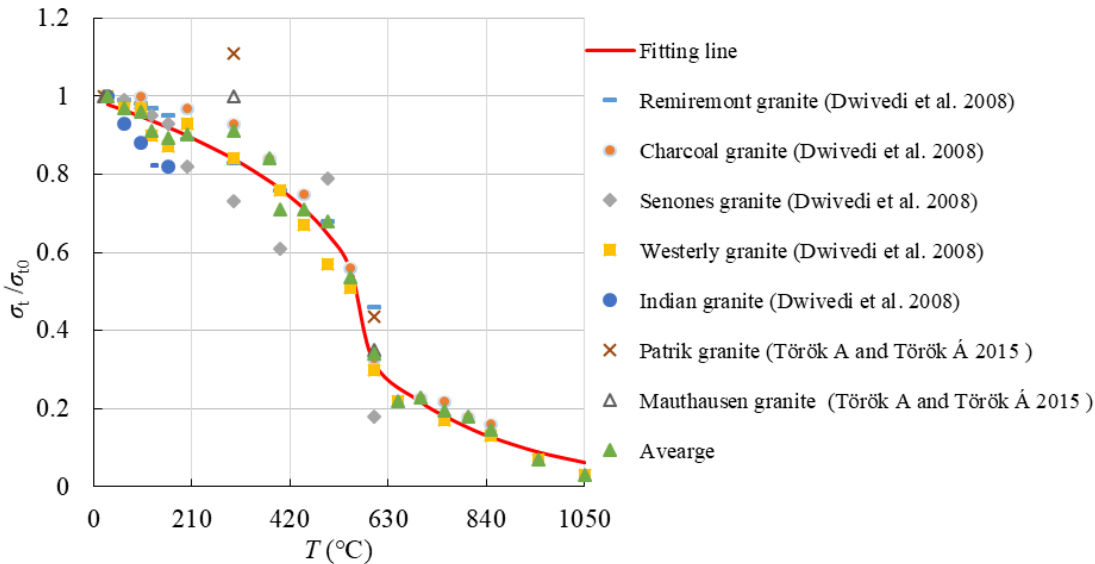


Fig. 3.5 Normalized tensile strength of granite samples vs. temperature (Wang and Konietzky, 2019)

### 3.5 Cohesion and friction angle

In general, cohesive strength will reduce at higher temperatures (see fig. 3.6), but the relationship between friction angle and temperature is hard to predict and very different for different rocks. In fig. 3.7, friction angles of different granites show a distinct different pattern at elevated temperatures. Compared with cohesion, the temperature dependency of friction angle is less significant and to some extent questionable (Wang and Konietzky, 2019). Heuze (1983) suggests at least a decay to zero towards the melting temperature of the rock.

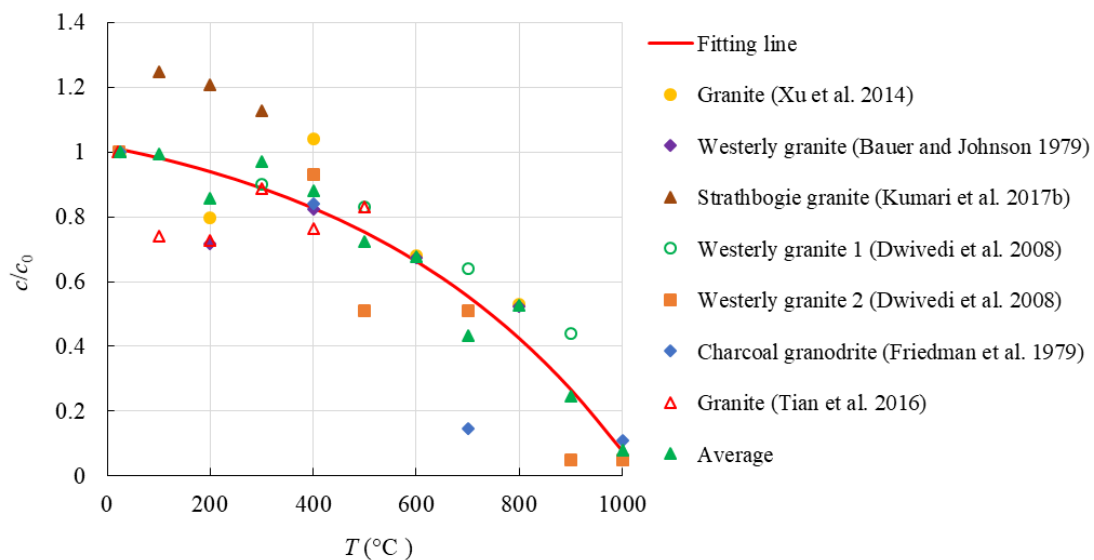


Fig. 3.6 Normalized cohesion of granites vs. temperature (Wang and Konietzky, 2019)

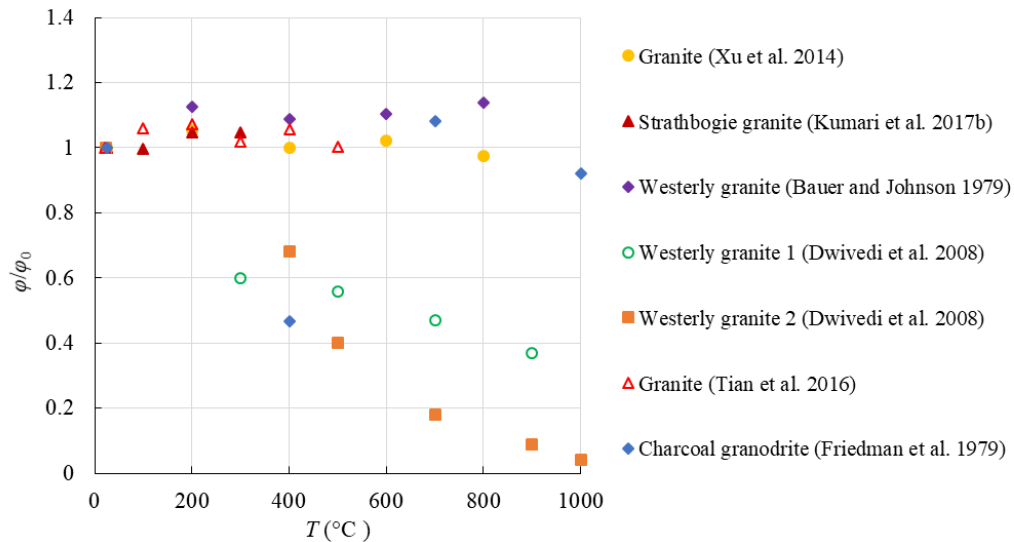


Fig. 3.7 Normalized friction angle of granites vs. temperature (Wang and Konietzky, 2019)

### 3.6 Young's modulus and Poisson's ratio

Development of Young's modulus with increasing temperature can also be quite different as shown in fig. 3.8. Some rocks exhibit a clear decrease in elastic modulus at elevated temperatures, while some rocks firstly experience a slight increase within a certain temperature range (e.g. 25 – 200  $^{\circ}\text{C}$ ). But for all rocks, elastic modulus will finally decrease to a much lower level after critical temperatures (e.g. 600  $^{\circ}\text{C}$ ).

Poisson's ratio decreases slightly with increasing temperature between 25  $^{\circ}\text{C}$  and 400  $^{\circ}\text{C}$  (fig. 3.9). However, the value might increase strongly beyond a critical temperature (e.g. 600  $^{\circ}\text{C}$ ). But this trend is not yet profound due to limited available experimental data beyond 600  $^{\circ}\text{C}$  and might be different for different types of rock.

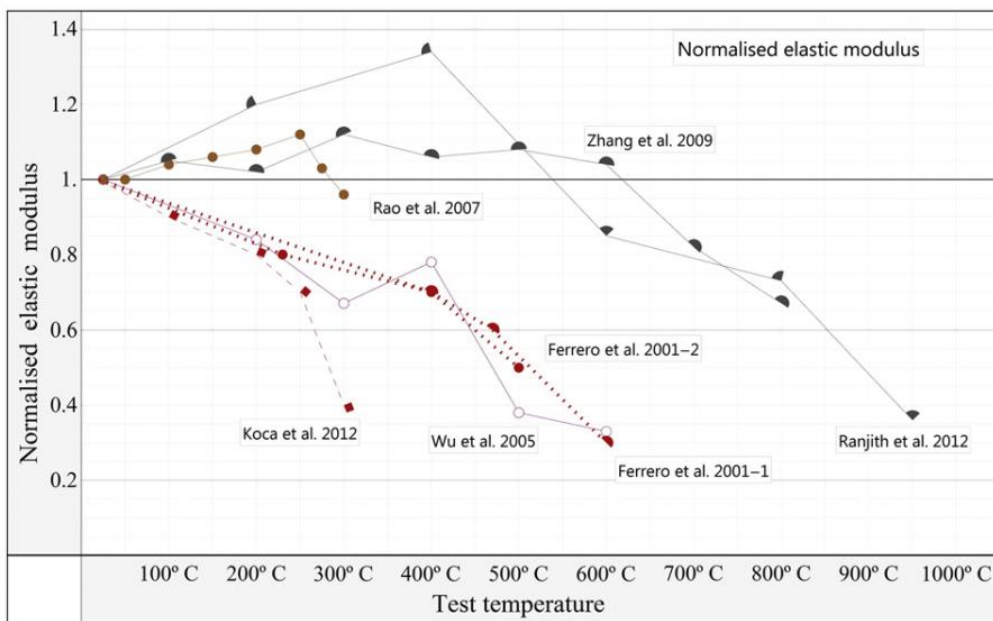


Fig. 3.8 Normalized elastic modulus vs. temperature after heat treatment (Brotóns et al., 2013)

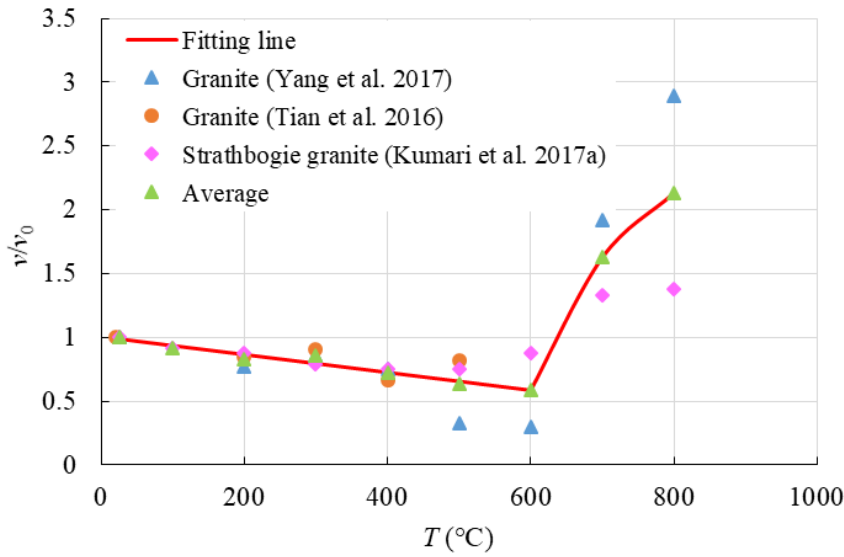


Fig. 3.9 Normalized Poisson's ratio of granites vs. temperature (Wang and Konietzky, 2019)

### 3.7 Linear thermal expansion coefficient

Thermal expansion is the tendency of matter to change in shape, area, and volume in response to a change in temperature. Different rocks have different expansion coefficients (see tab. 2). The values of coefficient of linear thermal expansion for granites increase with temperature and pressure, and they are strongly reduced beyond the  $\alpha$ - $\beta$  transition temperature of quartz (fig. 3.10).

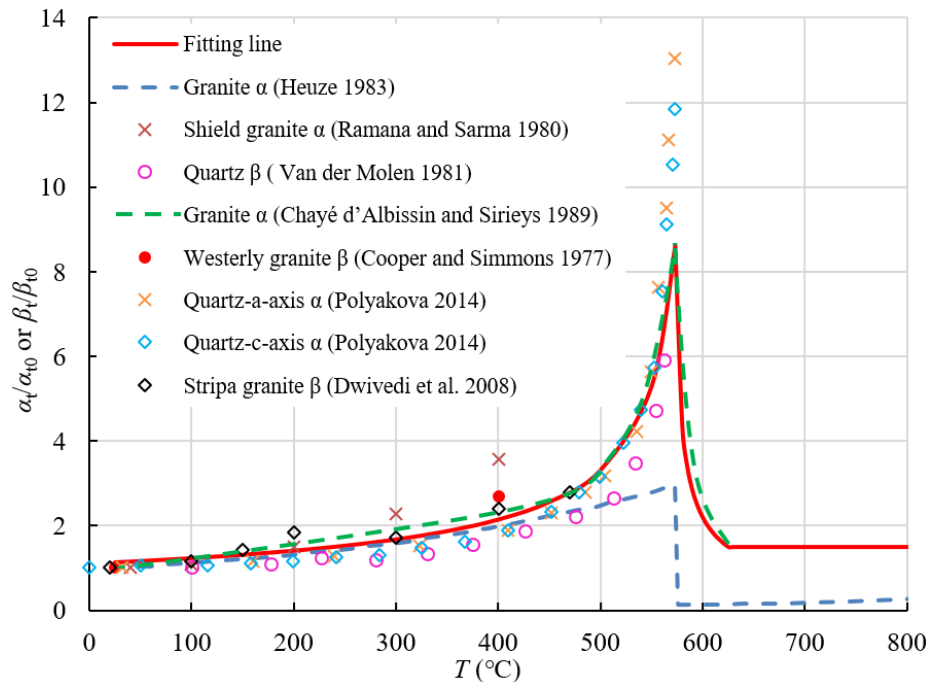


Fig. 3.10 Normalized thermal expansion coefficient of granites vs. temperature:  $\alpha$  and  $\beta$  means linear and volumetric values, respectively (Wang and Konietzky, 2019)

Tab. 2 Thermal expansion coefficients for several rock types (Siegesmund et al., 2011)

Rock class	Rock type	Linear expansion coefficient [ $10^{-6} \text{ K}^{-1}$ ]		
		Average	Max	Min
Magmatic	8 rock types	7.4	10	5
Metamorphic	marbles	11	15	8
	gneiss, schist	7.9	9	6
	quarzitic rocks	12.5	14	11
Sedimentary	calcareous sandstones	7.5	8	7
	limestones	4	6	2
	travertine	5	6	4
	sandstones	10.8	12	9.5

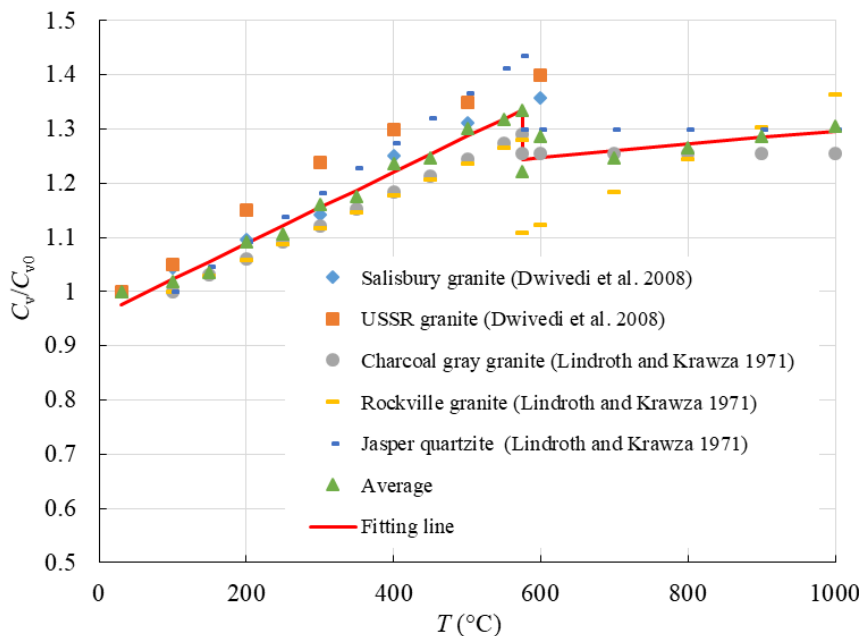


Fig 3.11 Normalized specific heat of granite samples vs. temperature (Wang and Konietzky, 2019)

### 3.8 Specific heat capacity

Fig. 3.11 shows that values of specific heat increase with temperature for all granites, but again some discontinuity is observed by the  $\alpha$ - $\beta$  transition of quartz at around 600°C.

### 3.9 Thermal conductivity

Thermal conductivities of crystalline rocks decrease with increased temperature. In general, the higher the conductivity of the rock, the greater is the decrease with increasing temperature. On the basis of lab test results for seven granites an empirical correlation has been developed (Heuze, 1983; Dwivedi et al., 2008) for the temperature range 30 °C to 300 °C:

$$k = 2.63 - 2.80 \cdot 10^{-3} T + 1.43 \cdot 10^{-6} T^2, \tag{6}$$

where  $k$  is in  $W/(m \cdot ^\circ C)$  and  $T$  is the temperature in °C.

From Fig. 3.12, we can see that the empirical law proposed by Heuze is also suitable for higher temperatures.

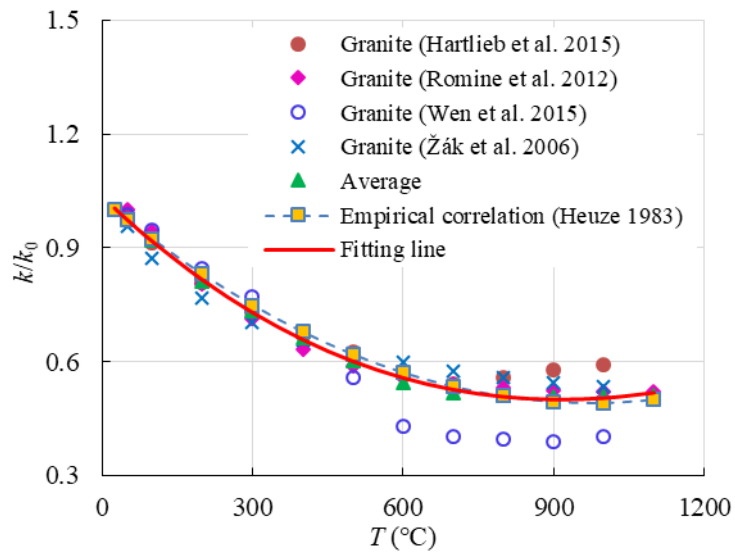


Fig. 3.12 Normalized thermal conductivity of granites vs. temperature (Wang and Konietzky, 2019)

## 4 Applications

### 4.1 Thermo-mechanical coupled modelling of granite specimen

A cylindrical granite specimen, 50 mm in diameter and 100 mm in length (Fig. 4.1), is heated in all directions. Because the sample is completely symmetric, only one quarter is used for simulation with two perpendicular symmetry planes. The bottom is fixed in vertical direction. All temperature-dependent parameters are assigned heterogeneously like shown exemplary in fig. 4.2 for the tensile strength. The sample is heated starting from room temperature (25 °C) at a constant heating rate (e.g. 5 °C/min).

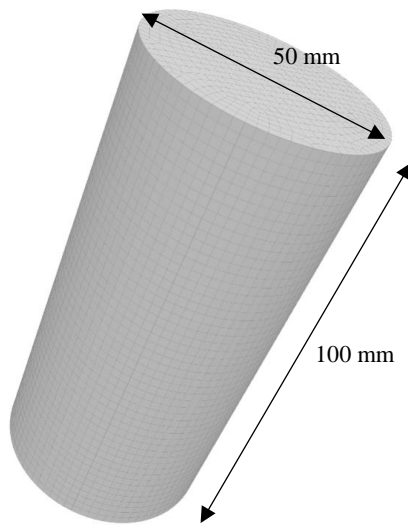


Fig.4.1 Schematic diagram of the granite model

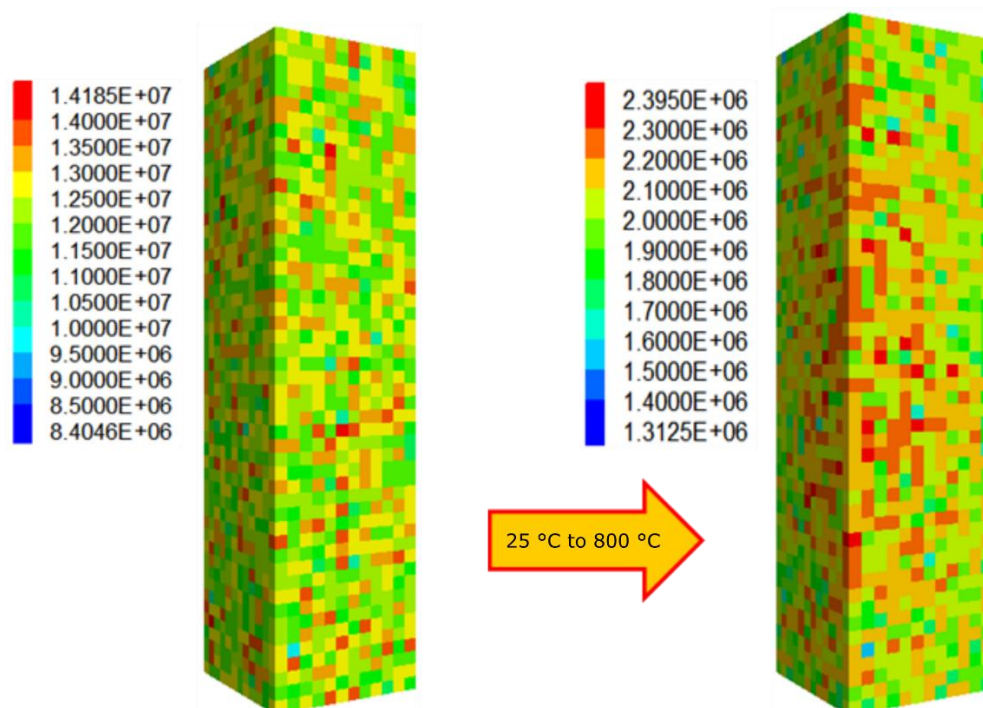


Fig. 4.2 Distribution of temperature-dependent tension strength (other parameters show similar pattern).

Fig. 4.3 shows the temperature distribution of the sample with temperature-dependent parameters. The temperature along the scanline is also plotted. When the sample boundary is heated to 800 °C, the maximum temperature difference between the boundary and the centre is about 22 °C.

Exemplary, Fig. 4.4 shows the positions of thermally induced cracks (elements with tensile and/or shear failure) after heating to about 400 °C, 600 °C and 800 °C. Thermal induced damage leads to softening like illustrated in Fig. 4.5, which shows simulated stress-strain curves for rock samples under uniaxial compression after heating up to certain temperatures.

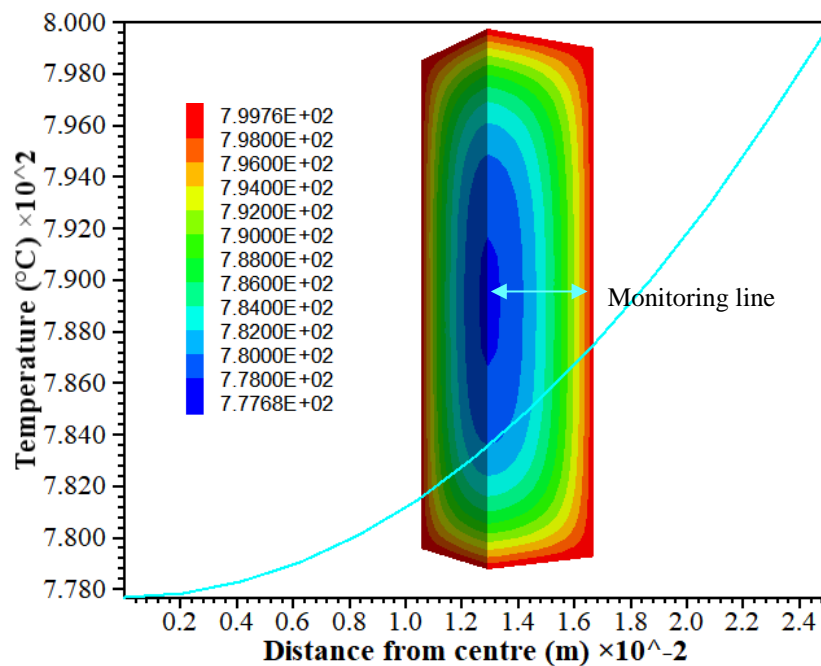


Fig. 4.3 Temperature distribution within the sample with temperature-dependent parameters

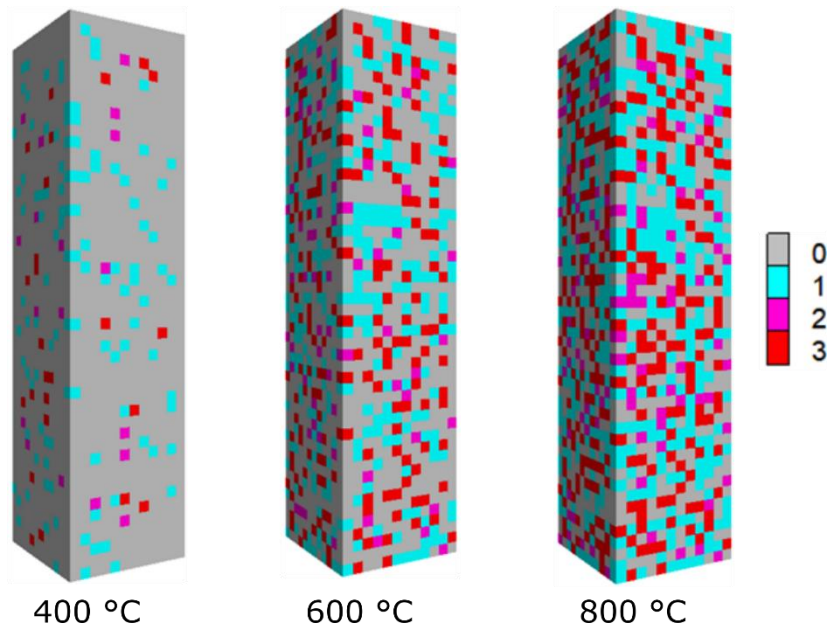


Fig. 4.4 Failed zones (0: undamaged, others: different damage types) in a heterogeneous granite sample after heating to certain temperatures

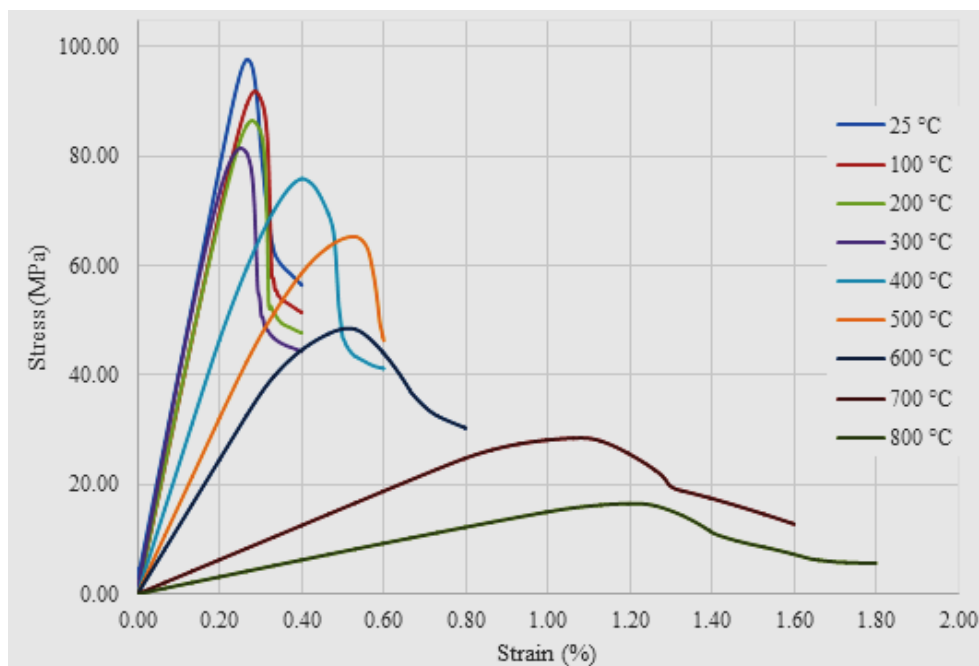


Fig. 4.5 Simulated stress-strain curve for uniaxial compression test on granite samples heating up to certain temperatures according to Fig. 4.4

#### 4.2 Thermo-mechanical coupled behaviour of heated porous rock sample

This example shows thermo-mechanical coupled simulations of a Voronoi-body based discrete element model (Fig. 4.6) for sandstone. Due to temperature distribution thermal cracking is observed as shown in Fig. 4.7. It has to be mentioned that this modelling is performed at the grain size level and pores are filled with an artificial injection material with different thermal expansion coefficient.

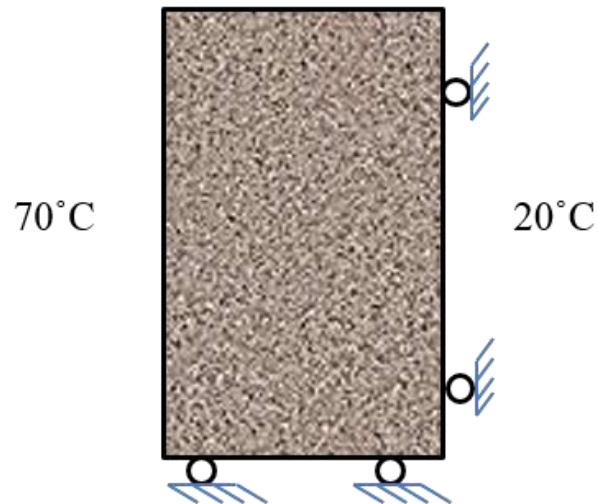


Fig. 4.6 Illustration of mechanical and thermal boundary conditions

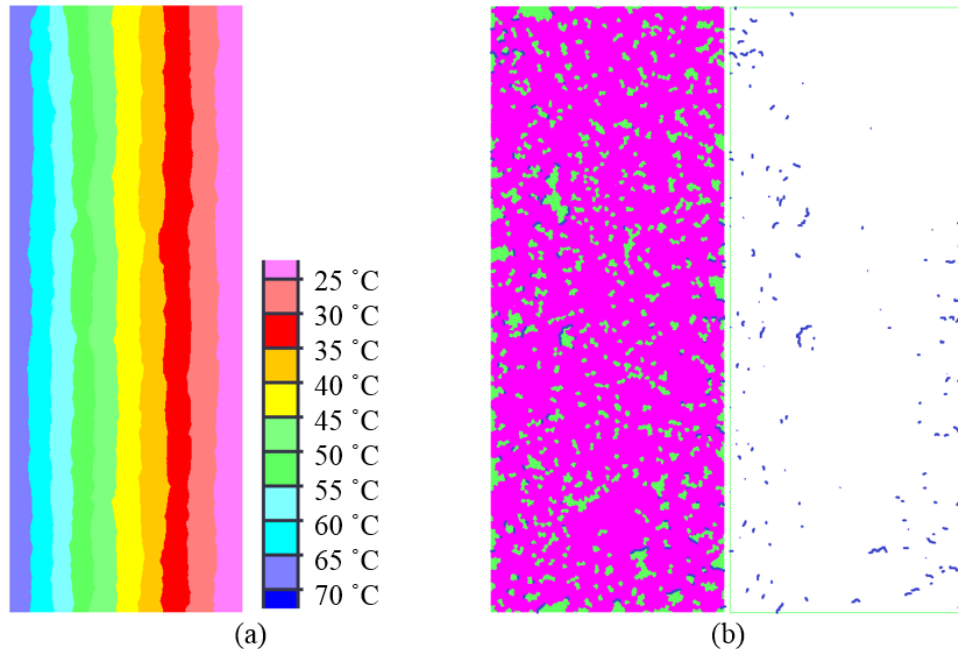


Fig. 4.7 (a): Temperature distribution and (b): crack pattern at thermo-mechanical equilibrium (cyan: rock matrix, green: pore filling, blue: cracks) (Li, 2017)

### 4.3 Example: Thermo-mechanical coupled behaviour of a rock sculpture

This example is a fundamental numerical study about the behaviour of a rock monument exposed to extreme sunshine. A heating up to 50°C is assumed. The sculpture consists of a pedestal and monument upon it. The sandstone monument has fillings with larger thermal expansion coefficient (rock:  $\alpha = 1 \cdot 10^{-7} \text{ K}^{-1}$ , filling:  $\alpha = 6.5 \cdot 10^{-7} \text{ K}^{-1}$ ). This produces compressive stresses (pressure) inside the fillings, but tensile stresses at the periphery. These tensile stresses can produce tensile cracks and fractures depending on tensile strength and fracture toughness of the rock, respectively. Note, that an additional mechanical vertical compression acts at the pedestal.

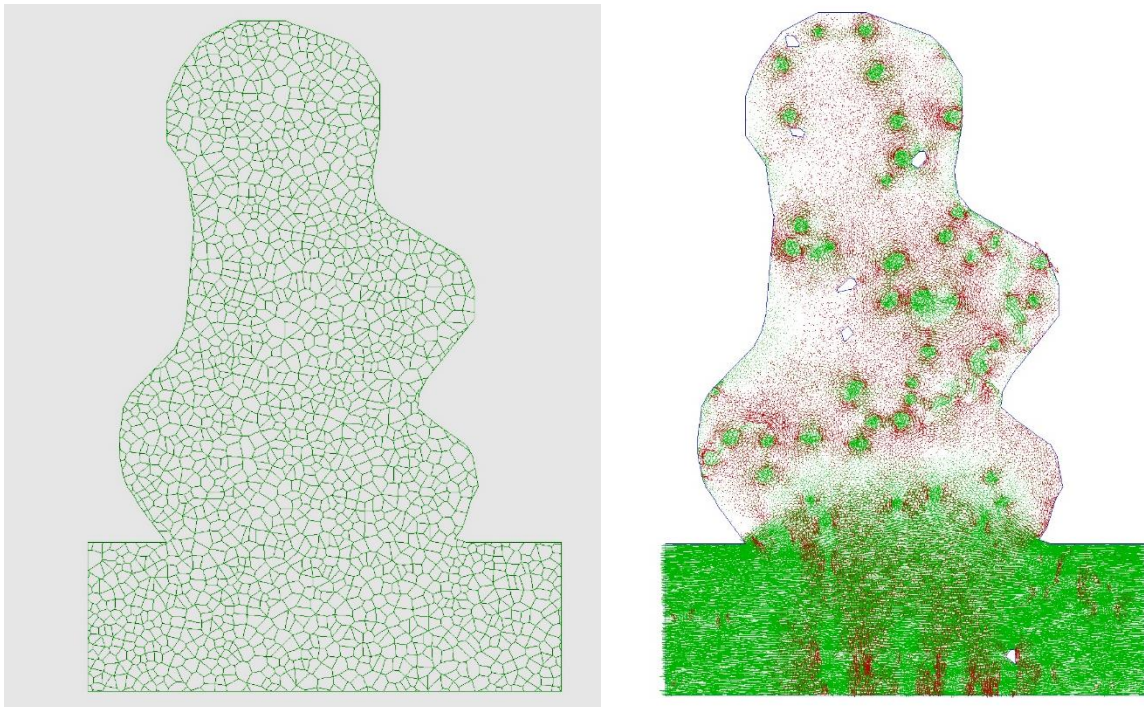


Fig. 4.8: Thermal stresses in a stone monument after heating to 50°C (left: Voronoi structure of numerical model; right: principal stresses after heating – green: compressive stresses, red: tensile stresses)

#### 4.4 Thermo-mechanical coupled simulation of high-level waste storage facility

TM- and HTM-coupled simulations are used to investigate the impact of heat production by high-level nuclear waste stored in underground repositories. The radioactive decay will produce heat for a long time, which will produce thermal induced stresses and deformations, but also additional pore water pressure. Fig. 4.9 shows the temperature distribution for a large scale model of a fictitious repository with 13 storage chambers several 100 meters below surface (left side of the model is a symmetry plane). Below the temperature development for selected observation points underground is shown.

#### 4.5 Thermo-mechanical simulations of rock behaviour for underground coal gasification

A coupled thermo-mechanical model has been developed to assess permeability changes in the vicinity of an underground coal gasification reactor resulting from excavation and thermo-mechanical effects (Otto and Kempka, 2015). Simulation results demonstrate that thermo-mechanical rock behaviour is greatly influenced by temperature-dependent parameters, but only insignificant differences in spatial permeability development are observed (Fig. 4.10).

#### 4.6 Thermo-mechanical behaviour of rock salt

A thermo-mechanical benchmark for a heated borehole (Fig. 4.11) was conducted. The particular aim of this work was to check and compare the description of the temperature dependence of transient and steady-state creep of rock salt with the involved constitutive models.

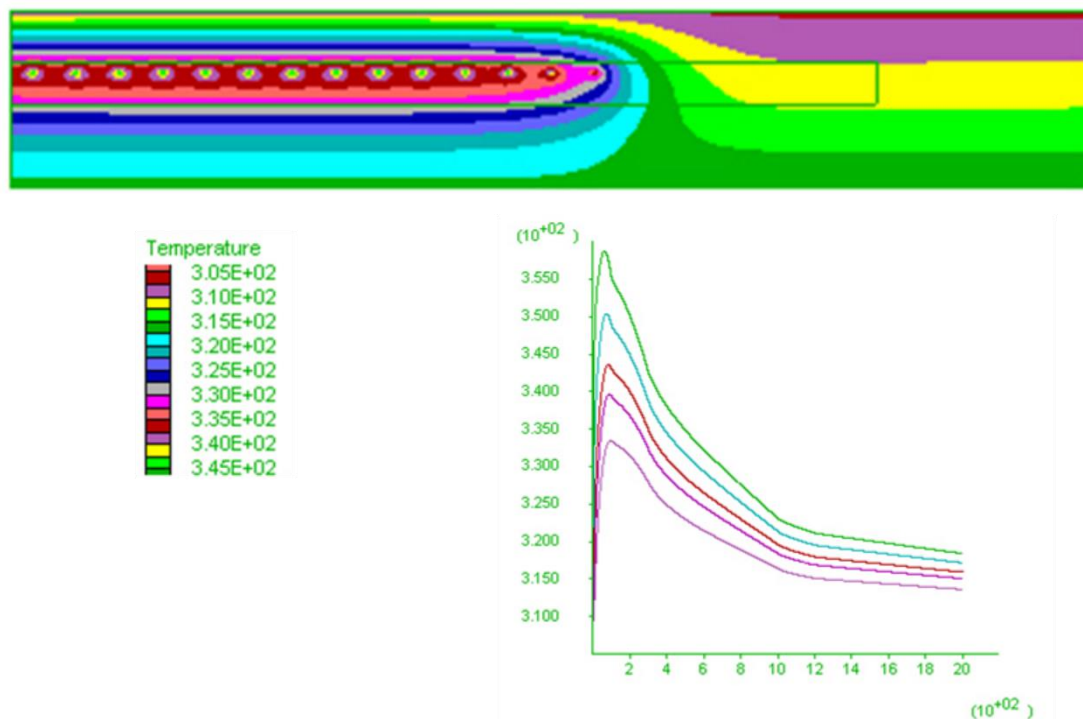


Fig. 4.9: Temperature development in a hypothetical underground nuclear repository for high-level waste. Top: temperature field (K) 100 years after emplacement of waste, bottom right: temperature development (K) versus time (years) for several observation points in different distance to the waste packages.

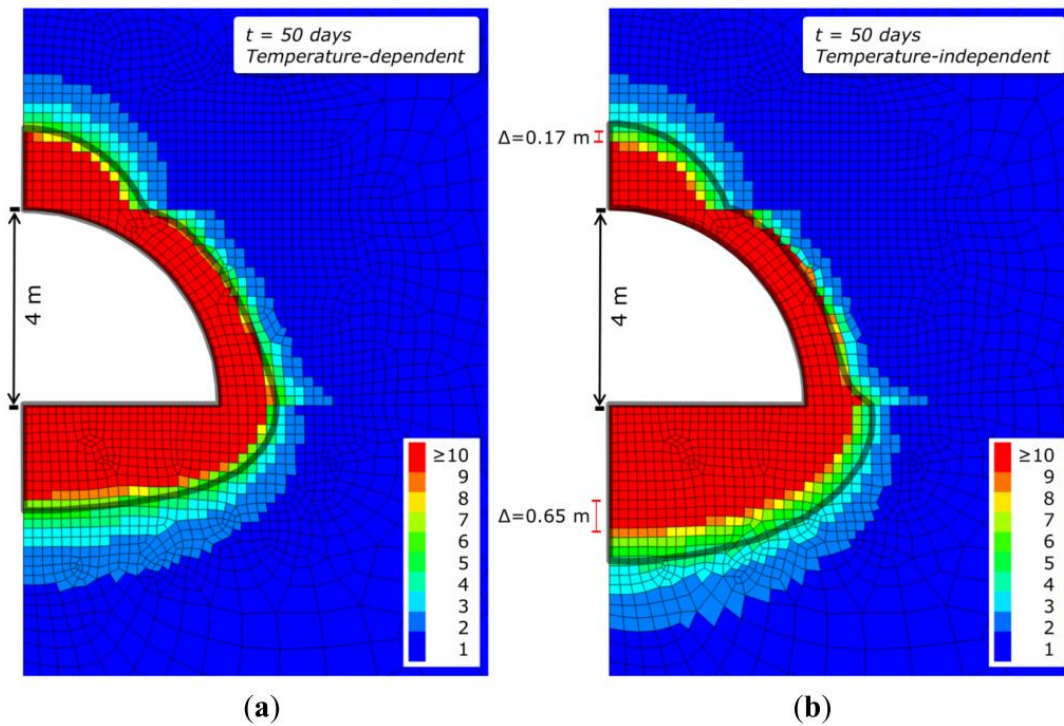


Fig. 4.10 Permeability changes show negligible differences for (a) temperature-dependent and (b) temperature-independent parameters. The difference in regions of high permeability increase is only marginal, extending to 0.17 m above and 0.65 m below the reactor. The grey solid line represents the 200 °C isotherm (Otto and Kempka, 2015).

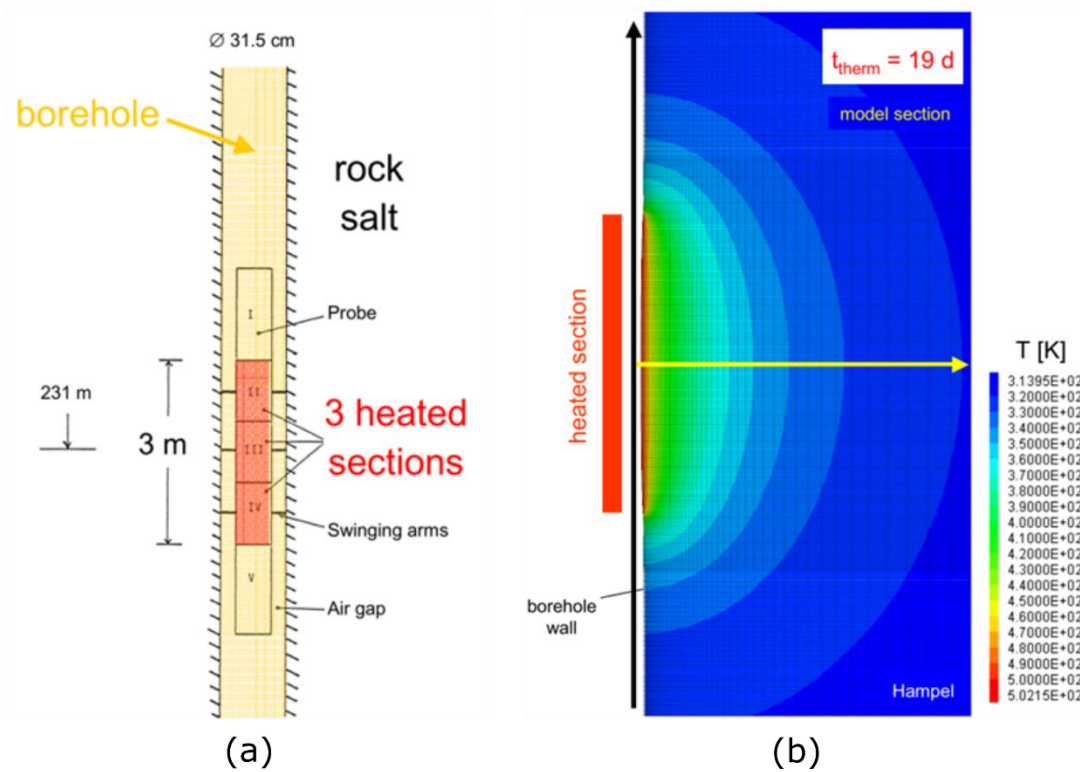


Fig. 4.11 Benchmark calculations of the heated borehole: (a) Illustration of the Heated Free Convergence Probe (HFCP) in the borehole, (b) calculated temperature distribution at the end of heating (day 19) in a model section around the heated zone of the borehole wall (Hampel, 2013)

## 5 References

- Brotóns V., Tomás, R., Ivorra S., and Alarcón J. C. (2013): Temperature Influence on the Physical and Mechanical Properties of a Porous Rock: San Julian's Calcarene. *Engineering Geology* 167: 117–27
- Chen, Y. and Wang, C. (1980): Thermally Induced Acoustic Emission in Westerly Granite. *Geophysical Research Letters* 7 (12): 1089 – 92.
- Dwivedi, R. D., Goel, R. K., Prasad, V. V R, and Amalendu, S. (2008): Thermo-Mechanical Properties of Indian and Other Granites. *International Journal of Rock Mechanics and Mining Sciences* 45 (3): 303 –15.
- Guha Roy, D. & Singh, T.N. (2016): Effect of Heat Treatment and Layer orientation on the Tensile Strength of Crystalline Rock Under Brazilian Test Condition. *Rock Mech. Rock Eng.* 49 (5): 1663-1677.
- Hampel, A. (2013): Benchmark Calculations of the Thermo-Mechanical Behavior of Rock Salt – Results from a US-German Joint Project. *47th US Rock Mechanics / Geomechanics Symposium*.
- Heap, M. J., Y. Lavallée, A. Laumann, K. U. Hess, P. G. Meredith, D. B. Dingwell, S. Huismann, and F. Weise. (2013): The Influence of Thermal-Stressing (up to 1000 °c) on the Physical, Mechanical, and Chemical Properties of Siliceous-Aggregate, High-Strength Concrete. *Construction and Building Materials* 42: 248 – 65.
- Heuze, F.E. 1983: High Temperature Mechanical, Physical and Thermal Properties of Granitic Rocks— A Review. *International Journal of Rock Mechanics and Mining Sciences & Geomechanics Abstracts* 20 (1): 3 –10.
- Li, J. (2017): Thermo-mechanical coupled damage behavior of pre-damaged rock sculptures and monuments - Laboratory Experiments and Numerical Simulations, PhD-Thesis, Geotechnical Institute, TU Bergakademie Freiberg
- Lindroth, D. P. (1974): Thermal diffusivity of six igneous rocks at elevated temperatures and reduced pressures. *U.S. Bureau of Mines Report of Investigations*, RI-7954.
- Liu, X., Zhang, C., Yuan, S., Fityus, S., Sloan, S.W., and Buzzi, O. (2016): Effect of High Temperature on Mineralogy, Microstructure, Shear Stiffness and Tensile Strength of Two Australian Mudstones. *Rock Mechanics and Rock Engineering* 49 (9): 3513 –24.
- Otto, C., and Kempka, T. (2015): Thermo-Mechanical Simulations Confirm: Temperature-Dependent Mudrock Properties Are Nice to Have in Far-Field Environmental Assessments of Underground Coal Gasification. *Energy Procedia* 76: 582 – 91.

- Shao, S., Ranjith, P. G., Wasantha, P. L.P., and Chen, B. K. (2015): Experimental and Numerical Studies on the Mechanical Behaviour of Australian Strathbogie Granite at High Temperatures: An Application to Geothermal Energy. *Geothermics* 54.: 96 –108.
- Siegesmund, S. (2011): Weathering and Deterioration. In: *Stone in Architecture*, Springer, 227 – 316.
- Tian, H., Mei, G., Zheng M. (2016): Rock properties after High Temperature Treatment (Book in Chinese).
- Tian, H., Kempka, T., Xu, N., and Ziegler, M. (2012): Physical Properties of Sandstones after High Temperature Treatment. *Rock Mechanics and Rock Engineering* 45 (6): 1113 –17.
- Wang, F., Konietzky, H. (2019): Thermo-Mechanical Properties of Granite at Elevated Temperatures and Numerical Simulation of Thermal Cracking. *Rock Mech Rock Eng*. DOI: 10.1007/s00603-019-01837-1.
- Xu, X.L, Gao, F., Zhang, Z.Z. (2014): Research on triaxial compression test of granite after high temperatures. *Rock and Soil Mechanics* 35(11): 3177 – 83.
- Yang, S.Q., Ranjith, P.G., Jing, H.W., Tian, W.L. and Ju, Y. (2017): An Experimental Investigation on Thermal Damage and Failure Mechanical Behavior of Granite after Exposure to Different High Temperature Treatments. *Geothermics* 65: 180 – 97